



# CHORUS

This is the accepted manuscript made available via CHORUS. The article has been published as:

## High-spin structure of $^{104}\text{Pd}$

D. Sohler *et al.*

Phys. Rev. C **85**, 044303 — Published 2 April 2012

DOI: [10.1103/PhysRevC.85.044303](https://doi.org/10.1103/PhysRevC.85.044303)

# High-spin structure of $^{104}\text{Pd}$

D. Sohler<sup>1</sup>, I. Kuti<sup>1</sup>, J. Timár<sup>1</sup>, P. Joshi<sup>2</sup>, J. Molnár<sup>1</sup>, E. S. Paul<sup>3</sup>, K. Starosta<sup>4,5</sup>, R. Wadsworth<sup>2</sup>, A. Algora<sup>1,6</sup>, P. Bednarczyk<sup>7</sup>, D. Curien<sup>8</sup>, Zs. Dombrádi<sup>1</sup>, G. Duchene<sup>8</sup>, D. B. Fossan<sup>4</sup>, J. Gál<sup>1</sup>, A. Gizon<sup>9</sup>, J. Gizon<sup>9</sup>, D. G. Jenkins<sup>2</sup>, K. Juhász<sup>10</sup>, G. Kalinka<sup>1</sup>, T. Koike<sup>4,11</sup>, A. Krasznahorkay<sup>1</sup>, B. M. Nyakó<sup>1</sup>, P. M. Raddon<sup>2</sup>, G. Rainovski<sup>12</sup>, J. N. Scheurer<sup>13</sup>, A. J. Simons<sup>2</sup>, C. Vaman<sup>14</sup>, A. R. Wilkinson<sup>2</sup>, L. Zolnai<sup>1</sup>

<sup>1</sup>*Institute of Nuclear Research, H-4001 Debrecen, Pf. 51, Hungary,*

<sup>2</sup>*Department of Physics, University of York, York YO10 5DD, UK,*

<sup>3</sup>*Oliver Lodge Laboratory, Department of Physics,*

*University of Liverpool, Liverpool L69 7ZE, UK,*

<sup>4</sup>*Department of Physics and Astronomy, State University of New York at Stony Brook, Stony Brook, New York 11794-3800, USA,*

<sup>5</sup>*Department of Chemistry, Simon Fraser University, Burnaby, British Columbia V5A 1S6, Canada,*

<sup>6</sup>*Instituto de Física Corpuscular, 46071 Valencia, Spain,*

<sup>7</sup>*GSI, Darmstadt, Germany,*

<sup>8</sup>*IReS, 23 rue du Loess, Strasbourg, 67037, France,*

<sup>9</sup>*LPSC, IN2P3-CNRS/UJF, F-38026 Grenoble-Cedex, France,*

<sup>10</sup>*Department of Information Technology, University of Debrecen, H-4032 Debrecen, Hungary,*

<sup>11</sup>*Graduate School of Science, Tohoku University, Sendai, 980-8578, Japan,*

<sup>12</sup>*Faculty of Physics, St. Kliment Ohridski University of Sofia, BG-1164 Sofia, Bulgaria,*

<sup>13</sup>*Université Bordeaux 1, IN2P3- CENBG - Le Haut-Vigneau BP120 33175, Gradignan Cedex, France,*

<sup>14</sup>*NSCL, Cyclotron Laboratory, Michigan State University, East Lansing, MI 48824-1321, USA*

High-spin structure of the nucleus  $^{104}\text{Pd}$  was studied through the  $^{96}\text{Zr}(^{13}\text{C},5n)$  reaction at incident energies of 51 and 58 MeV, using the EUROBALL IV  $\gamma$ -ray spectrometer in conjunction with the DIAMANT charged particle array. Several new medium- and high-spin bands were revealed. The already known positive-parity yrast and the negative-parity cascades were extended up to  $E_x \sim 13$  MeV,  $\sim 11$  and  $\sim 9$  MeV with  $I^\pi=(26^+)$ ,  $I^\pi=(23^-)$  and  $(20^-)$ , respectively. The deduced band structures were compared with Woods-Saxon TRS calculations. In addition, non-yrast low-lying positive-parity bands were identified, which were assigned to soft  $\gamma$ -vibrational excitations.

PACS numbers: 21.10.Hw,21.60.Ev,23.20.Lv,27.60.+j

## I. INTRODUCTION

Transitional nuclei lying in the  $A \sim 100$  mass region have been in the forefront of nuclear structure research during the last decades. These investigations have revealed large variety of interesting phenomena related to triaxial nuclear shapes such as the occurrence of signature inversion in  $^{98,100-103}\text{Rh}$  [1], the appearance of chiral twin bands in  $^{104-106}\text{Rh}$  [2–4] and the identification of quasi- $\gamma$  band in  $^{102}\text{Ru}$ , the core nucleus of  $^{104}\text{Rh}$  [5]. Recently, studying the chiral doublet bands in  $^{103}\text{Rh}$  it has been shown that the energy separation of these structures depends mainly on the core properties and to a lesser extent on the valence quasiparticle coupling [6]. However, the chiral interpretation in the  $A = 130$  region has been questioned by lifetime measurements [7, 8], and it could not be confirmed either by lifetime experiment in the nuclei  $^{103}\text{Rh}$  and  $^{104}\text{Rh}$  [9]. In this respect, it is important to understand the necessary conditions leading to the emergence of chiral geometry, one of which is the shape of the corresponding even-even core. Mapping the border of chirality in this region, the structure of  $^{105}\text{Ag}$ , the even-even core of which is  $^{104}\text{Pd}$ , has also been investigated, nevertheless, no chiral side band to the yrast band could be found [10]. Furthermore, the properties of the chiral-candidate doublet band structure in  $^{106}\text{Ag}$

can be explained in terms of increased gamma softness [11] compared to that of observed in  $^{104}\text{Rh}$ . It is, therefore, interesting to investigate if this difference is also reflected in the core nuclei  $^{104}\text{Pd}$  and  $^{102}\text{Rh}$ . In order to answer this question, we studied the high- and medium-spin structure of  $^{104}\text{Pd}$ .

Concerning the lowest-energy excited bands,  $^{104}\text{Pd}$  is expected to show very similar characteristics to that of its neighbouring even-even isotone  $^{102}\text{Ru}$ . In the latter nucleus several two-quasiparticle bands have been established [12] and thus appearance of similar structures is expected in  $^{104}\text{Pd}$ , too.

Collective and two-quasiparticle excitations in  $^{104}\text{Pd}$  have been previously studied via the  $^{94}\text{Zr}(^{13}\text{C},3n\gamma)$  reaction by Grau *et al.* [13]. High angular momentum, positive- and negative-parity states have been identified in this work using excitation function,  $\gamma$ -ray angular distribution,  $\gamma$ -ray linear polarization and  $\gamma\gamma$ -coincidence measurements. The observed states have been interpreted with the help of a slightly deformed rotor description in terms of the interacting boson model. A more precise linear polarization measurement of  $\gamma$  rays assigned to  $^{104}\text{Pd}$  have been performed by Stromswold *et al.* [14] using a Compton calorimeter. Their linear polarization results clearly showed the negative parity for the two major sidebands. Moreover, a high-spin rotational band has

been found in this nucleus by Macchiavelli *et al.* and interpreted as arising from superdeformed shapes [15].

Recently, candidate chiral structures in the rhodium isotopes around  $A \sim 104$  were studied by in-beam  $\gamma$ -spectroscopy [3, 4]. In the performed experiment we collected a significant amount of data also on  $^{104}\text{Pd}$ , making it possible to extend its band structure. Section II presents the experimental techniques, data evaluation and results, followed by the interpretation of the experimental findings in section III.

## II. EXPERIMENTAL METHODS AND RESULTS

High-spin states in  $^{104}\text{Pd}$  were populated using the  $^{96}\text{Zr}(^{13}\text{C},5n)$  fusion-evaporation at beam energies of 51 and 58 MeV. The  $^{13}\text{C}$  beam, provided by the the Vivitron accelerator at IReS, Strasbourg, impinged on a stack of two targets, each of thickness  $558 \mu\text{g}/\text{cm}^2$  and enriched to 86% in  $^{96}\text{Zr}$ . The emitted  $\gamma$  rays were detected by the EUROBALL IV detector array [16] equipped with 15 cluster [17] and 26 clover [18] composite Ge detectors. The cluster detectors were placed at backward angles, while the clover detectors were positioned in two rings at an averaged angle of  $90^\circ$  relative to the beam direction. The  $\gamma$  rays were measured in coincidence with light charged particles in order to eliminate the contaminants from reaction channels produced by evaporation of protons and  $\alpha$ -particles from the  $^{109}\text{Pd}$  compound nuclei. The detection of charged particles was performed by means of the highly efficient DIAMANT array which was consisted of 88 CsI detector elements [19]. Protons and  $\alpha$ -particles were used as veto.

A total of  $\sim 2 \times 10^9$  triple- and higher-fold coincidence events were accumulated and stored onto magnetic tapes among which  $\sim 4.5 \times 10^8$  belonged to the  $^{104}\text{Pd}$  reaction channel. The data obtained from the Ge detectors were sorted off-line into a 3-dimensional histogram by requiring non-detection of any charged particle. For the analysis of the triple-coincidence cube a standard gating procedure was carried out with the help of the RADWARE software package [20]. Sample  $\gamma$ -ray gated spectra are shown in Fig. 1.

The  $\gamma$ -ray energies and relative intensities, derived from the  $\gamma\gamma\gamma$ -coincidence cube, are listed in Table I. The Ge detectors were calibrated for both energy and efficiency by using a  $^{152}\text{Eu}$  source placed at the target position. The systematic errors due to the energy and efficiency calibrations were estimated to be  $\sim 0.2$ - $0.3$  keV and  $\sim 5\%$ , respectively. Altogether 104 transitions were assigned to  $^{104}\text{Pd}$ , 56 of which are observed the first time in the present work.

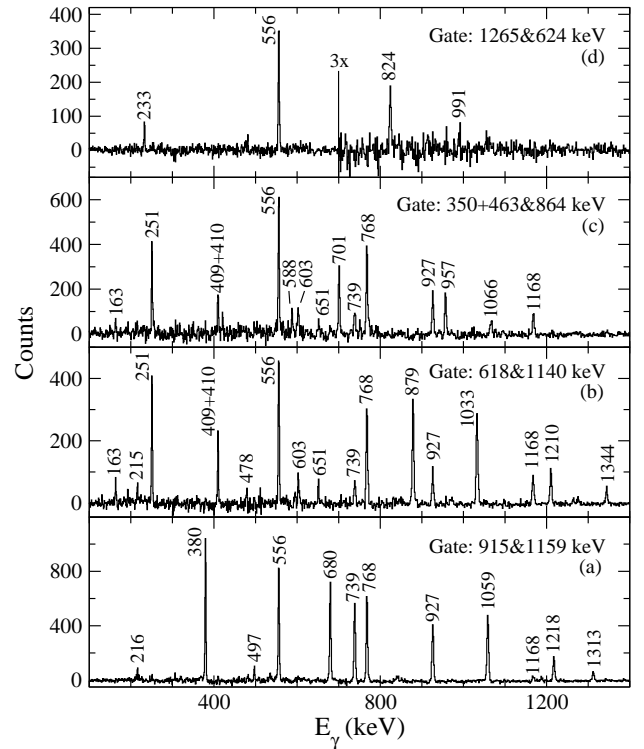


FIG. 1: Typical background subtracted  $\gamma\gamma\gamma$ -coincidence spectra showing the placement of band 3 (a), band 4 (b), band 6 (c) and band 7 (d), respectively. Double gates are indicated on the panels.

TABLE I: Energies, relative intensities, DCO ratios, linear polarisations, and deduced multipolarities of transitions assigned to  $^{104}\text{Pd}$  in the present work.

$E_\gamma$ (keV)	$I_\gamma$ (rel.)	$R_{\text{DCO}}$	P	Mult.	$E_i$ (keV)
116.1(4)	0.5(1)	0.64(22)		D	2298
163.1(3)	3.9(2)	0.43(6)		D	3152
193.0(3)	2.1(3)	0.66(10)		D	2492
193.6(4)	0.4(1)	0.98(16)		Q	3152
200.9(3)	1.2(2)	1.04(12)		$D^\alpha$	3422
215.4(4)	1.5(2)	1.08(14)		$D^\alpha$	2298
215.9(4)	1.6(1)				3368
233.2(6)	0.3(1)	0.61(12)		D	2678
233.3(5)	0.7(1)	0.57(9)		D	2901
250.9(3)	7.8(5)	1.09(8)	0.33(23)	E2	3152
309.7(5)	0.7(1)	0.98(12)		Q	2492
320.8(6)	1.0(1)	1.01(13)	0.72(46)	E2	2989
349.9(3)	1.2(2)	0.97(10)		$D^\alpha$	3502
361.5(5)	0.5(1)	0.59(11)		D	2445
371.2(5)	0.2(1)	1.05(20)		$D^\alpha$	3593
379.6(3)	22.3(14)	1.04(6)	0.65(9)	E2	3368
401.4(4)	1.2(1)	0.50(6)	-0.41(23)	M1	3770
408.7(8)	0.2(1)	0.60(12)			2492
409.6(4)	6.1(4)	0.67(7)	-1.21(86)	M1	2901
427.7(5)	0.8(1)	1.08(19)		$D^\alpha$	2678
462.6(3)	0.5(1)	0.52(12)	-0.87(66)	M1	4203
467.2(6)	2.3(2)	0.65(7)	-0.84(36)	M1	2959
469.3(4)	0.3(1)	0.44(11)		D	5433
477.7(5)	1.0(2)				2298

TABLE I: continued

$E_\gamma$ (keV)	$I_\gamma$ (rel.)	$R_{\text{DCO}}$	P	Mult.	$E_i$ (keV)
478.8(8)	0.6(1)				1821
497.4(3)	2.3(2)	1.00(8)	0.55(22)	E2	2989
505.8(4)	0.5(1)				6528
513.0(5)	0.6(1)				3502
535.1(7)	0.7(1)	0.50(11)		D	5067
543.2(8)	0.2(1)				3502
555.9(3)	100.0(61)	1.01(5)	0.46(5)	E2	556
573.5(3)	0.2(1)				9191
587.6(3)	1.1(1)	0.55(8)	0.61(44)	E1	4636
587.9(3)	1.6(2)	0.59(7)	-1.15(55)	M1	3740
590.7(5)	0.8(1)				3269
594.6(3)	0.2(1)				10468
595.2(4)	2.0(2)				2678
600.3(5)	1.0(1)	0.60(7)		D	4649
601.3(3)	2.4(2)	1.04(9)	0.25(8)	E2	4024
602.9(3)	3.9(3)	0.99(7)	0.35(8)	E2	2901
612.0(3)	18.8(12)	1.02(5)	0.50(7)	E2	4636
617.7(3)	8.1(6)	1.08(7)	0.45(8)	E2	3770
623.7(4)	1.1(2)	1.11(18)		Q	2445
650.8(3)	3.0(3)	1.03(8)		D <sup>a</sup>	2901
655.4(4)	0.8(1)	0.65(8)	0.76(26)	E1	4024
666.5(4)	0.3(1)	0.63(12)		D	4259
674.8(4)	0.2(1)				8099
679.8(3)	15.9(11)	1.00(5)	0.60(9)	E2	4048
700.6(4)	1.3(2)	1.08(14)	0.95(50)	E2	4203
718.2(4)	0.2(1)	0.70(12)		D	5682
738.6(3)	31.6(20)	0.51(4)	0.37(6)	E1	2989
741.3(4)	1.3(2)	0.94(17)		Q	2083
748.0(8)	0.3(1)	0.99(18)		D <sup>a</sup>	7108
751.0(3)	1.1(1)	1.07(12)	0.53(11)	E2	3740
758.9(6)	0.9(1)	1.09(21)		D <sup>a</sup>	2083
762.0(3)	1.1(1)				4532
767.9(3)	92.8(43)	1.02(6)	0.54(6)	E2	1324
785.9(3)	1.0(1)				1342
791.9(4)	1.9(2)				4532
794.0(4)	0.8(1)	0.96(12)		D <sup>a</sup>	6227
797.3(3)	13.3(12)	1.02(6)	0.76(12)	E2	5433
802.6(3)	22.1(15)	0.96(5)	0.63(8)	E2	4024
824.5(8)	0.4(1)	0.95(20)		Q	3269
858.1(6)	2.5(2)	0.53(6)		D	2182
864.0(4)	1.1(2)	1.02(17)		Q	5067
879.0(3)	6.3(3)	1.08(8)	0.67(11)	E2	4649
914.5(5)	1.0(2)	0.99(16))		Q	3593
915.4(3)	10.2(8)	1.03(8)	0.46(14)	E2	4964
926.6(3)	73.6(49)	1.05(6)	0.61(7)	E2	2250
926.9(3)	8.9(6)	0.98(7)	0.69(20)	E2	6360
955.8(7)	0.8(1)				5488
957.0(4)	1.4(2)				6024
971.2(3)	28.8(18)	0.94(5)	0.57(8)	E2	3222
974.5(3)	1.5(2)	1.07(18)		D <sup>a</sup>	2298
990.6(7)	0.4(1)	1.02(21)		Q	4259
990.9(8)	0.2(1)				8099
1019.3(4)	1.6(2)	0.97(10)	0.25(18)	E2	4241
1021.9(8)	0.5(1)				7550
1026.4(5)	0.5(1)	1.03(21)		Q	4619
1032.9(3)	3.9(3)	1.04(8)	0.47(18)	E2	5682
1040.6(6)	0.6(1)				6528
1058.7(3)	6.8(5)	0.97(7)	0.74(28)	E2	6022
1063.8(3)	6.3(5)	1.04(8)	0.76(18)	E2	7424
1066.4(5)	0.7(1)				7090
1076.2(6)	0.3(1)				8166

TABLE I: continued

$E_\gamma$ (keV)	$I_\gamma$ (rel.)	$R_{\text{DCO}}$	P	Mult.	$E_i$ (keV)
1140.5(3)	2.1(2)	0.97(10)	0.74(53)	E2	6822
1147.9(5)	0.4(1)				5389
1159.1(3)	3.3(2)	0.98(7)	0.75(24)	E2	7182
1167.8(3)	13.8(8)	0.51(4)	0.42(19)	E1	2492
1172.5(4)	4.4(3)	0.99(7)	0.99(33)	E2	3422
1193.3(3)	3.3(3)	1.04(8)	0.91(39)	E2	8617
1210.5(4)	0.8(1)	1.02(23)	1.13(57)	E2	8033
1217.9(3)	1.2(2)	1.02(12)	0.65(38)	E2	8399
1256.2(3)	1.5(2)	1.02(11)	0.65(36)	E2	9873
1264.8(4)	2.1(2)	0.67(7)	-0.40(25)	M1	1821
1312.9(6)	0.5(1)	1.05(20)	1.20(80)	E2	9712
1342.1(7)	0.4(1)	1.08(19)	1.20(82)	E2	1342
1344.1(9)	0.2(1)	1.04(19)	0.65(52)	E2	9377
1344.4(6)	2.8(2)	0.58(6)	0.77(37)	E1	2668
1354.3(6)	1.0(2)	1.03(14)	1.21(64)	E2	2678
1365.2(4)	0.4(1)	1.01(19)		Q	11239
1385.7(7)	0.2(1)				11098
1468.4(6)	0.2(1)				12707
1527.0(3)	1.6(2)	0.93(14)	1.99(102)	E2	2083
1624.4(5)	0.8(1)				2182

<sup>a</sup> indicates non-stretched  $\Delta I=0$  dipole transition.

Information on the multipolarities of transitions with sufficient intensity was extracted from an analysis of directional correlation of oriented nuclei (DCO) ratios [21]. For the DCO analysis, data obtained from the cluster detectors mounted at an average angle of  $156^\circ$  and the clover detectors arranged at about  $90^\circ$  were used. A non-symmetric  $E_\gamma - E_\gamma$  matrix, comprising of the  $\gamma$  rays observed in the cluster detectors along one axis and the  $\gamma$  rays observed in the clover detectors along the other axis, was created by requiring non-detection of any charged particle. The ratios  $R_{\text{DCO}} = I_{\gamma\gamma}(156^\circ, 90^\circ[\text{gate}]) / I_{\gamma\gamma}(90^\circ, 156^\circ[\text{gate}])$  were extracted applying corrections for the different efficiencies of the clover and the cluster detector rings. Theoretical DCO ratios have been calculated for the experimental geometry as described in Ref. [3]. These estimates revealed that a value of  $R_{\text{DCO}}=1.0$  corresponds to a stretched quadrupole transition and  $\approx 0.6$  to a stretched dipole one, when the gating transition is a stretched quadrupole  $\gamma$  ray. For the used experimental geometry we can expect that  $R_{\text{DCO}}$  for a pure non-stretched dipole transition with  $\delta \approx 0$  multipole mixing ratio is approximately the same as for a stretched quadrupole transition. For mixed M1+E2 transitions  $R_{\text{DCO}}$  ratios can vary between 0.5 and 1.0 depending on the  $\delta$  mixing ratio of the  $\gamma$  ray [3]. The attenuation coefficients of incomplete alignment were fitted to strong transitions with known multipolarities in the calculations.

The DCO ratios obtained in this way for already known transitions of  $^{104}\text{Pd}$  are consistent with the previous assignments of Grau *et al.* [13] and Stromswold *et al.* [14] except for some minor differences. Grau *et al.* assigned  $\Delta I=1$  M1+E2 multipolarity to the 350 keV transition, while we propose  $\Delta I=0$  dipole character for this  $\gamma$  ray. A stretched dipole character is obtained for the 858 keV

$\gamma$  ray from our experimental data, in contrast with the previous non-stretched M1 assignment of Grau *et al.*. The results of the DCO analysis are summarized in Table I.

The multipolarity assignments were further supported by deducing the electromagnetic character of the transitions by measuring the linear polarization of the  $\gamma$  rays. For this purpose, the four-element clover detectors placed close to  $90^\circ$  relative to the beam direction were used as Compton polarimeters [22]. Two matrices were constructed from  $\gamma\gamma$ -events detected in anti-coincidence with any charged particle; single hits in any  $\gamma$ -detector were placed on one axis while the added-back double-hit scattering  $\gamma$ -energies were placed on the other axis. In the first matrix the scattering events took place perpendicular, while in the second matrix parallel to the reaction plane. The number of perpendicular ( $N_\perp$ ) and parallel ( $N_\parallel$ ) scatters for a given  $\gamma$  ray were obtained from spectra gated on the single-hit axis of the respective matrix by transitions in coincidence with the given  $\gamma$  ray. Assuming that each clover crystal has equal efficiency, an experimental linear polarization is defined as

$$P = \frac{1}{Q} \frac{N_\perp - N_\parallel}{N_\perp + N_\parallel}, \quad (1)$$

where  $Q$  is the polarization sensitivity for the clover detectors, which is a function of the  $\gamma$ -ray energy [22].  $N_\perp$  and  $N_\parallel$  denote the number of events scattered perpendicular and parallel to the reaction plane, respectively.  $P > 0$  is characteristic for stretched E1, E2 and non-stretched M1 transitions, while  $P < 0$  characterizes stretched M1 and non-stretched E1 transitions. The linear polarisation ratios obtained for the previously known transitions of  $^{104}\text{Pd}$  are in agreement with the earlier assignments of Stromswold *et al.* [14]. The results of the linear polarisation analysis are given in Table I.

During the multipolarity assignments only dipole and electric quadrupole transitions were considered. In addition, it was assumed that in the heavy-ion induced fusion-evaporation reactions, high-spin states are preferably populated and their decays proceed mainly via stretched transitions along the yrast line. Therefore, we assigned the maximum possible spin value allowed by the angular distribution ratios of the transitions to the states. Definite parity was proposed to a state if E1, M1 or quadrupole character could be determined for one of the transitions connecting it to a state with known parity. The multipolarities obtained are listed in Table I.

### A. The level scheme of $^{104}\text{Pd}$

The proposed level scheme shown in Fig. 2 was constructed using the  $E_\gamma - E_\gamma - E_\gamma$  coincidence relations, energy and intensity balances. The order of the transitions in the  $\gamma$ -ray cascades was deduced from the intensity relations when no other information was available. The placement of the known transitions is consistent with the

previous works [13–15] except that our coincidence data did not support the existence of the 941 keV  $\gamma$  ray assigned to  $^{104}\text{Pd}$  by Grau *et al.* [13]. The already known bands (*bands 1, 3, 4, 8*) were extended to higher excitation energy and spin. In addition, several new bands (*bands 5, 6, 7, 9*) were observed and linked to the previously reported ones.

The yrast *band 1* has been previously reported up to  $8 \hbar$  [13–15]. In the present work it was extended up to an excitation energy  $E_x = 5.4$  MeV with two additional levels decaying by the 1019 and the 1148 keV transitions. The deduced multipolarities are in agreement with the known spin-parity values for this band, thus we adopt these values up to  $I^\pi = 8^+$ . On the basis of the DCO and linear polarization analysis, stretched E2 is assigned to the 1019 keV  $\gamma$  ray suggesting  $I^\pi = 10^+$  value for the state at 4241 keV. The 1148 keV  $\gamma$  ray is too weak to obtain information on its multipolarity. As this  $\gamma$  ray continues the rotational sequence, it is assumed to be a stretched E2 transition and a tentative  $I^\pi = (12^+)$  spin-parity value is assigned to the state at 5389 keV.

*Band 2* has been previously observed up to  $I^\pi = (16^+)$  in Ref. [14],  $I^\pi = 18^+$  in Ref. [13] and  $I^\pi = (26^+)$  in Ref. [15]. Our experimental data confirmed the previous placements of the transitions assigned to this band and the spin-parity values of the levels up to  $I^\pi = 18^+$ . From the DCO and linear polarization data stretched E2 and quadrupole character are deduced for the 1193, 1256 and the 1365 keV  $\gamma$  rays, respectively, resulting in unambiguous  $I^\pi = 20^+, 22^+$  and  $24^+$  spin-parities for the states at 8617, 9873 and 11239 keV. The intensity of the 1468 keV  $\gamma$  ray is not sufficient to draw a conclusion about its multipolarity, so the spin-parity assignment of the level at 12707 keV remains tentative.

The lower part of *band 3* up to  $I^\pi = 15^-$  has been identified in Refs. [13, 14]. Our coincidence data support the previous placements of the transitions assigned to this band and allow the extension of the band structure by four levels up to an excitation energy  $E_x \approx 11.1$  MeV. In Fig. 1 a) the sum of triple  $\gamma$ -ray gate spectra shows clearly all the transitions placed in this cascade except for the gating 915 and 1159 keV  $\gamma$  lines. The extracted multipolarities are in accordance with the former spin-parity assignments of *band 3* up to  $I^\pi = 15^-$ . On the basis of the deduced stretched E2 characters of the 1159, 1218 and 1313 keV  $\gamma$  rays, we propose  $17^-, 19^-$  and  $21^-$  spin-parity values for the levels at 7182, 8399 and 9712 keV. The 1386 keV  $\gamma$  ray is too weak to determine its multipolarity. However, since this transition continues the rotational structure, a tentative  $I^\pi = (23^-)$  spin-parity value is proposed to the state at 11098 keV.

*Band 4* has been reported up to  $I^\pi = 14^-$  by Grau *et al.* [13] and Stromswold *et al.* [14]. The observed coincidence relations strengthen the positions of the 233, 410, 603, 651, 163, 251, 401, 618, 879 and 1033 keV  $\gamma$  rays. Two more linking transitions to *band 3* with energies of 718 and 600 keV were found and *band 4* was extended by three states which decay by the 1140, 1210

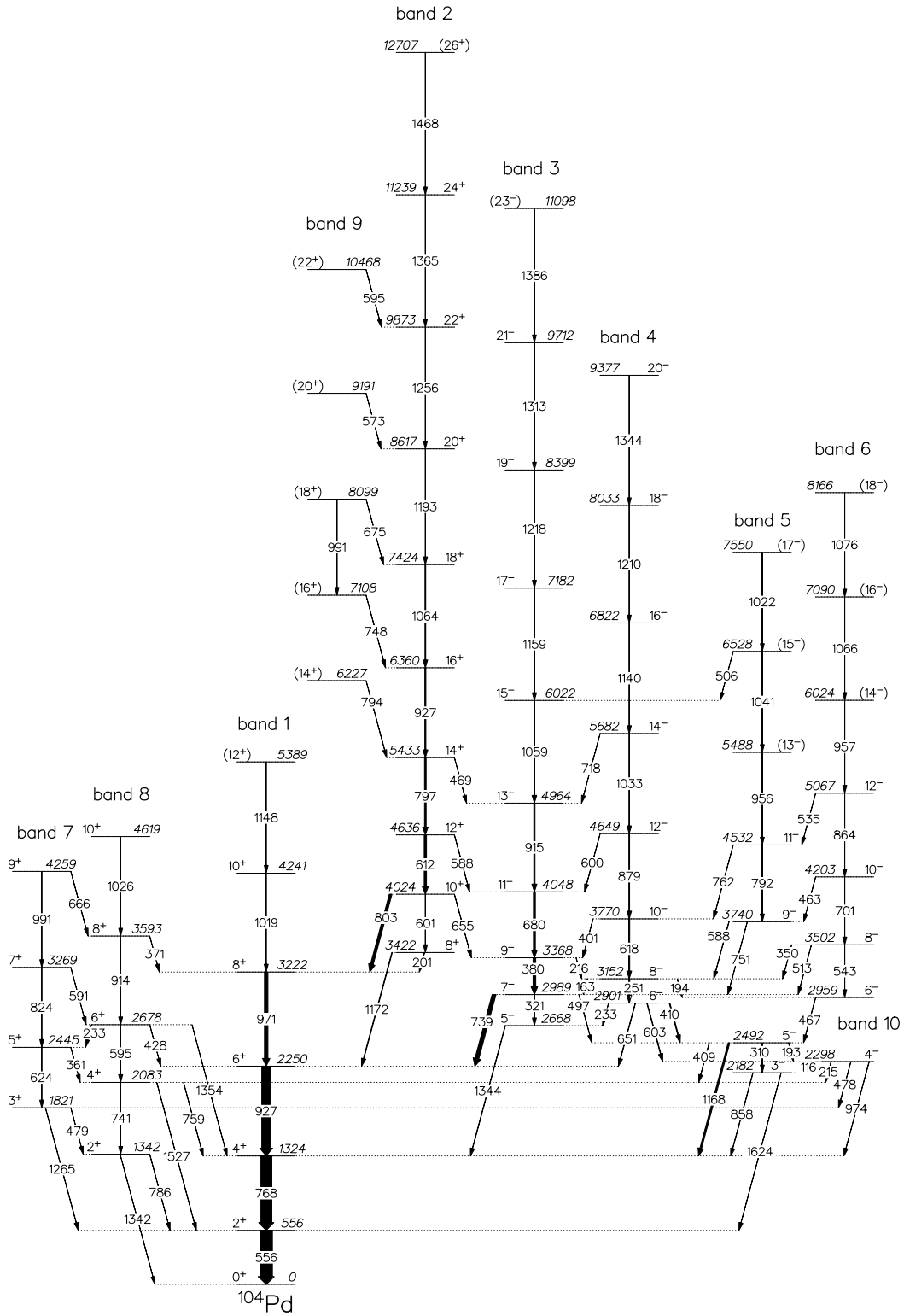


FIG. 2: The partial level scheme of  $^{104}\text{Pd}$  obtained in the present work.

and 1344 keV  $\gamma$  rays as it is shown in Fig. 1 b). The multiplicities obtained for the transitions placed in the lower part of the band are in agreement with the previous spin-parity assignments [13, 14]. Above the  $I^\pi=14^-$  state, the stretched E2 multipolarity of the 1140, 1210 and 1344 keV transitions yields the spin-parity assignments of the  $16^-$ ,  $18^-$  and  $20^-$  states.

The lowest-lying negative parity states at 2182, 2298 and 2492 keV have been established by Refs. [13, 14]. Our experimental data confirm the stretched E1 multipolarity for the 1168 keV  $\gamma$  ray suggested by Stromswold *et al.* [14] and, thus, the firm  $I^\pi=5^-$  assignment for the 2492 keV initial state.  $I^\pi=4^+$  and  $4^-$  spin-parity values have been proposed by Grau *et al.* [13] to the states at 2182 and 2298 keV, respectively. The stretched E2 character obtained for the 603 keV transition, which connects the  $I^\pi=6^-$  2901 keV and the 2298 keV states, strengthens the  $I^\pi=4^-$  assignment to the latter one. The 2182 keV level is fed by the 116 and 310 keV  $\gamma$  rays from the  $3^-$  and  $5^-$  states at 2298 and 2492 keV, as well as connected by the 858 and 1624 keV transitions to the yrast  $2^+$  and  $4^+$  states. The stretched quadrupole character of the 310 keV  $\gamma$  ray deduced from our DCO data suggests a  $I^\pi=3^-$  spin-parity to the 2182 keV state contrary to the  $4^+$  value of Grau *et al.* [13]. Our assignment is supported by the stretched dipole character obtained for the 116 and 858 keV transitions.

Besides the major sideband structures, two new bands (*bands 5* and *6*) were found to decay to the negative-parity states. On the basis of the coincidence relations *band 5* is connected to *bands 3* and *4*, among others, by the M1 588 keV and the E2 751 keV  $\gamma$  rays, thereby firmly establishing negative parity for *band 5*. The stretched quadrupole nature of the 751 keV and the stretched character of the 588 keV transitions determine the  $I=9$  spin assignment for the lowest level in the band at 3740 keV. The 762 and 792 keV  $\gamma$  rays, deexciting the next state in the band at 4532 keV, were too weak to determine their multiplicities. In order to deduce an unambiguous spin-parity of this level, the stretched dipole assignment of the 535 keV  $\gamma$  line was used. This transition feeds the 4532 keV state from the  $12^-$  5067 keV one, hence,  $I^\pi=11^-$  value is proposed to the final state. Due to the insufficient intensity of the 956, 1041 and 1022 keV  $\gamma$  rays tentative  $I^\pi=(13^-)$ ,  $(15^-)$  and  $(17^-)$  values are assigned to the higher observed levels in *band 5*.

In *band 6* Grau *et al.* have been identified the lowest-lying 467, 350 and tentatively the 701 keV  $\gamma$  rays to  $^{104}\text{Pd}$  [13]. Based on the coincidence relations, shown in Fig. 1 c), we assigned these transitions to a rotational structure, which was extended by four additional transitions up to an excitation energy  $E_x \approx 8.2$  MeV and connected to *bands 4* and *5* by three more  $\gamma$  rays. In the case of the 467 keV transition a stretched M1 multipolarity was obtained establishing a firm  $I^\pi=6^-$  spin-parity for the lowest level in the band at 2959 keV. The 4203 keV state is connected by the stretched M1 463 keV  $\gamma$  ray to the  $9^-$  state in *band 5*, thus,  $I^\pi=10^-$  value is assigned to

this level. The  $I^\pi=8^-$  spin-parity of the middle-lying 3502 keV state was determined from the stretched E2 character of the feeding 701 keV transition. This assignment is confirmed by the  $\Delta I=0$  non-stretched dipole nature of the deexciting 350 keV  $\gamma$  line. Above the  $I^\pi=10^-$  state, the stretched quadrupole character of the 864 keV transition yields the spin-parity of the  $12^-$  state. The intensity of the 957, 1066 and 1076 keV  $\gamma$  rays are not sufficient to draw a conclusion about their multiplicities, so the spin-parity assignment of the levels at 6024, 7090 and 8166 keV remains tentative.

In addition to the already known positive-parity bands, there appeared three other rotational-like structures, *bands 7*, *8* and *9*, connected to this part of the level scheme. The 1265 keV  $\gamma$  ray linking the lowest-lying state in *band 7* to the yrast band has been observed by Grau *et al.* and a stretched M1 multipolarity has been assigned to it [13]. On the basis of our experimental data we confirmed the position of this transition and the  $I^\pi=3^+$  spin-parity of its initial state at 1821 keV. Using the observed coincidence relations, shown in Fig. 1 d), a new band was built on this state up to an excitation energy  $E_x \approx 4.3$  MeV. Based on the quadrupole character of the 624, 824 and 991 keV  $\gamma$  rays, we propose  $5^+$ ,  $7^+$  and  $9^+$  spin-parity values for the levels at 2445, 3269 and 4259 keV.

The yrare  $2^+$  and  $4^+$  states have been identified by Grau *et al.* [13]. Our coincidence data confirm the previous placements of the 1342, 786, 741, 1527 and 759 keV transitions, and make possible to extend the cascade by three levels and to connect to *band 1* and *7* by several transitions. The obtained stretched E2 and quadrupole multiplicities of the 1342, 1527 and 741 keV  $\gamma$  rays are in accordance with the spin-parities of the states at 1342 and 2083 keV, thus, we adopt the  $I^\pi=2^+$  and  $4^+$  values to them. On the basis of the DCO and linear polarization analysis, stretched E2 and quadrupole characters are deduced also to the 1354, 914 and 1026 keV transitions, respectively, suggesting unambiguous  $I^\pi=6^+$ ,  $8^+$  and  $10^+$  values for the states at 2678, 3593 and 4619 keV. The assignments in *band 7* and *8* are further corroborated by the  $\Delta I=1$  (233, 361, 666 keV  $\gamma$  rays) and the  $\Delta I=0$  (371, 428, 759 keV  $\gamma$  rays) dipole natures of the linking transitions.

In *band 9* mainly the linking transitions to *band 2* were observed. Unfortunately, these  $\gamma$  rays do not have enough intensity to get any information on their multiplicities. If we assigned stretched quadrupole character to them, these states would become yrast which contradicts the fact that this band is populated less than 10 times weaker than the yrast *band 2* at this spin region. Thus, we assume tentative  $I^\pi=(14^+)$ ,  $(16^+)$ ,  $(18^+)$ ,  $(20^+)$  and  $(22^+)$  spin-parity values for the states at 6227, 7108, 8099, 9191 and 10468 keV, respectively.

### III. DISCUSSION

The  $^{104}\text{Pd}$  nucleus with its six valence protons and eight valence neutrons lies in the upper part of the  $g_{9/2}$  proton subshell and in the middle part of the  $d_{5/2}$ ,  $g_{7/2}$  neutron subshell where the low- $\Omega$   $h_{11/2}$  orbitals intrude already at small deformations. According to previous studies [13, 14], *band 2*, *3* and *4* correspond to two-quasiparticle bands being built on the aligned positive-parity  $\nu(h_{11/2})^2$  and negative-parity  $\nu h_{11/2}$ , ( $d_{5/2}$ ,  $g_{7/2}$ ) configurations, respectively. To get a deeper insight into the structure of the observed bands, total routhian surface (TRS) calculations based on the Woods-Saxon cranking formalism [23–25] were performed and compared with Routhians ( $E'$ ) and aligned angular momenta ( $I_x, i_x$ ) [26].

In  $^{104}\text{Pd}$  at slight deformations the neutron Fermi surface located near the  $[411]3/2$  and  $[413]5/2$  positive-parity Nilsson states arising from the  $d_{5/2}$ ,  $g_{7/2}$  subshell, as well as the  $[550]1/2$  and  $[541]3/2$  negative-parity Nilsson states originating from the  $h_{11/2}$  orbital. With increasing rotational frequency the high- $j$  low- $\Omega$   $[550]1/2$  state moves closer to the Fermi surface, and thus this orbital is presumed to contribute to the lowest-energy excited rotational bands. These assumptions are in a good agreement with that both in  $^{103}\text{Pd}$  [27] and  $^{105}\text{Pd}$  [28] the two lowest-lying positive-parity bands are assigned to the  $d_{5/2}$ ,  $g_{7/2}$  origin, and the negative-parity band built on the  $h_{11/2}$  configuration becomes the yrast structure above  $I^\pi=(11^-)$ . Moreover, in  $^{105}\text{Pd}$  the alignment of the  $h_{11/2}$  neutron pair appears in higher-energy positive-parity states. The proton Fermi surface lies in the middle of the unique-parity  $g_{9/2}$  subshell, close to the  $[303]5/2$  and  $[301]1/2$  normal-parity Nilsson orbitals.

The  $i_x$  experimental alignments presented in Fig. 3, were deduced by subtracting a reference based on a variable moment of inertia  $J_{r,ef}=J_0+\omega^2 J_1$  with  $J_0=14 \hbar^2/\text{MeV}$  and  $J_1=15 \hbar^4/\text{MeV}^3$ . The  $K$  quantum number was taken to be 0 for the ground state band, since it corresponds to the quasiparticle vacuum configuration at low rotational frequency. *Bands 3*, *4*, *5* and *6* are considered as two-quasineutron configurations involving the  $[550]1/2$  and one of the  $[411]3/2$  or  $[413]5/2$  Nilsson orbitals, for which we assume to have  $K=1/2$ ,  $3/2$  and  $5/2$  values, respectively. Consequently, the possible  $K$  values for these bands are 1, 2 or 3, of which an average value of 2 was applied in calculating the alignments in accordance with Ref. [13]. We note that at higher spins the alignment of a band is not sensitive to varying the value of  $K$  by one or two units.

The positive-parity *band 2* of  $^{104}\text{Pd}$  has been assigned to the two-quasiparticle  $\nu(h_{11/2})^2$  configuration [13, 14]. According to this expectation, the alignment of a  $h_{11/2}$  neutron pair is clearly visible at  $\hbar\omega\approx 0.4$  MeV frequency in Fig. 3 with nearly the full possible alignment gain of  $\sim 10 \hbar$ . *Band 1* shows a small, about  $2 \hbar$  alignment at higher frequency of  $\sim 0.5$  MeV/ $\hbar$ , which might be a sign of the  $\pi(g_{9/2})^2$  alignment. Such an alignment is seen also for *bands 5* and  $6$  in good agreement with the corre-

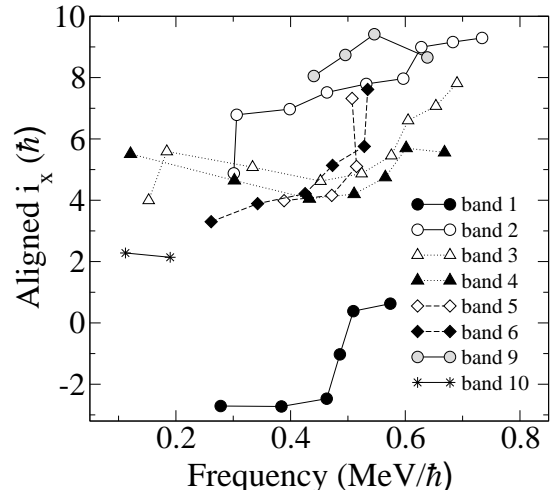


FIG. 3: Experimental alignments  $i_x$  of *bands 1-6* and *9*. A frequency-dependent moment-of-inertia reference was subtracted.

TABLE II: Labels used for the quasideuteron (p) and quasineutron (n) states for parity  $\pi$  and signature  $\alpha$  with  $n$  denoting the  $n^{\text{th}}$  such state.

p			n		
$(\pi, \alpha)_n$	label	Shell model	$(\pi, \alpha)_n$	label	Shell model
$(+, +1/2)_1$	a	$g_{9/2}$	$(+, +1/2)_1$	A	$d_{5/2}, g_{7/2}$
$(+, -1/2)_1$	b	$g_{9/2}$	$(+, -1/2)_1$	B	$d_{5/2}, g_{7/2}$
$(-, -1/2)_1$	e	$p_{1/2}$	$(+, +1/2)_2$	C	$d_{5/2}, g_{7/2}$
$(-, +1/2)_1$	f	$p_{1/2}$	$(+, -1/2)_2$	D	$d_{5/2}, g_{7/2}$
			$(-, -1/2)_1$	E	$h_{11/2}$
			$(-, +1/2)_1$	F	$h_{11/2}$
			$(-, -1/2)_2$	G	$h_{11/2}$
			$(-, +1/2)_2$	H	$h_{11/2}$

sponding TRS results. In *bands 3*, *4*, *5* and *6* the  $\nu h_{11/2}$  alignment seems to be blocked, as they do not show a similar alignment gain at  $\sim 0.4$  MeV/ $\hbar$ . This results in that their configuration contains one neutron in the  $h_{11/2}$  orbit. On the basis of the alignment curves these bands are supposed to be configured by two quasiparticles. Since the parity of these bands is negative, the second quasineutron is expected to have a  $g_{7/2}$ ,  $d_{5/2}$  origin.

According to these considerations, total routhian surface TRS calculations were performed for the vacuum and for two-quasiparticle configurations with one quasineutron in the  $h_{11/2}$  state and another one in the four lowest-energy positive-parity states. For labelling the lowest-energy quasineutron states the commonly used notations, given in Table II, are adopted.

#### A. The yrast positive-parity bands

The experimental Routhians ( $E'$ ) and the aligned angular momenta ( $I_x$ ) are compared with the results of the

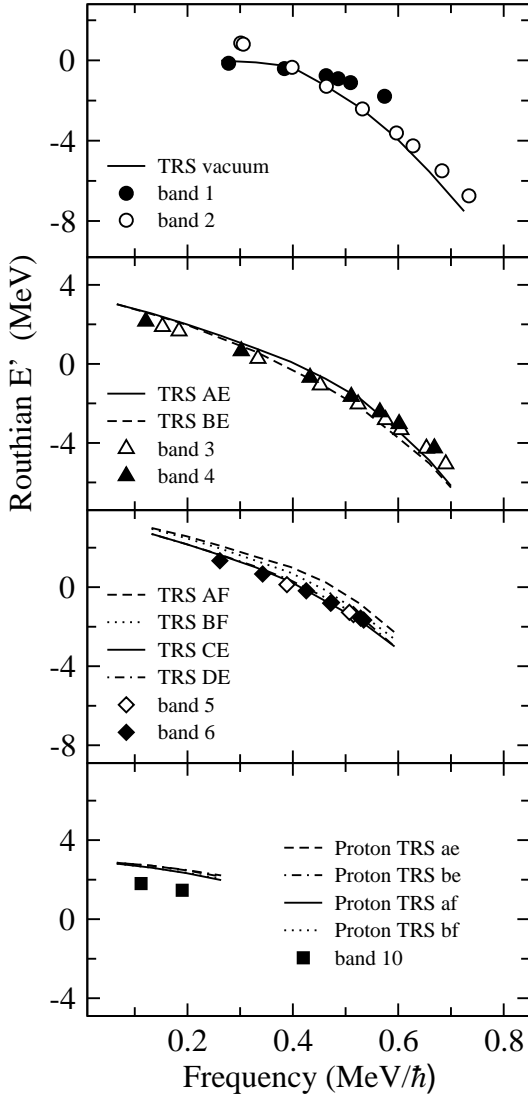


FIG. 4: Comparison of the experimental and TRS Routhians  $E'$  for bands 1-6 and 10.

TRS calculations in Fig. 4 and 5, respectively. The theoretical  $E'$  curves are normalized so that the experimental and the TRS Routhians of the yrast band overlap each other. The yrast sequence agrees well with the vacuum configuration of the TRS calculations before the first  $h_{11/2}$  neutron pair is aligned, while *band 2* corresponds with the vacuum configuration after this alignment. The TRS calculations give a good overall description of the Routhians and aligned angular momenta. The predicted shape for *band 1* starting from  $\hbar\omega \approx 0.3$  MeV is characterized by  $\beta_2 \approx 0.14$  and  $\gamma \approx -2^\circ$ , while the  $\nu(h_{11/2})^2$  alignment drives it to slightly larger  $\beta_2 \approx 0.19$  and  $\gamma \approx 5^\circ$  values for *band 2*.

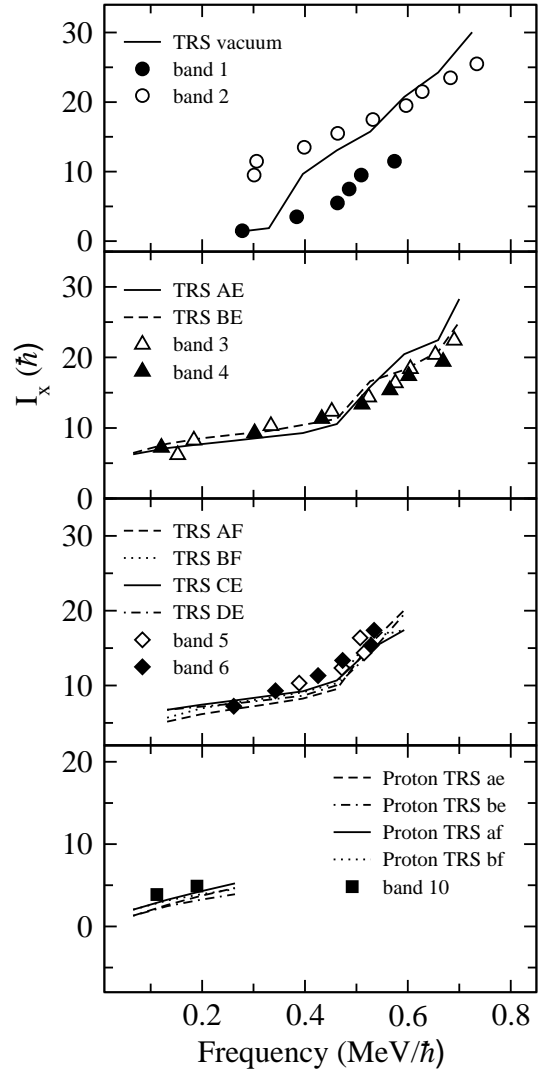


FIG. 5: Comparison of the experimental and TRS aligned angular momenta  $I_x$  for bands 1-6 and 10.

## B. The negative-parity bands

As it can be seen from the experimental alignments  $i_x$  of bands 3 and 4 in Fig. 3 and discussed before, the structure of these bands are determined by similar two-quasineutron configurations. The lowest energy negative-parity two-quasineutron configurations are expected to involve one quasineutron from the E  $h_{11/2}$  orbital and another quasineutron from the A or B  $d_{5/2}, g_{7/2}$  orbitals. Based on the good agreement between the experimental and the TRS Routhians (see Fig. 4), we suggest these coupled bands having  $\nu h_{11/2}, (d_{5/2}, g_{7/2})$  configuration.

The TRS calculations for aligned angular momentum predict the appearance of a proton alignment at about 0.53 MeV/h in the case of bands 3 and 4. In nuclei with  $A \sim 100$  below the  $Z=50$  shell closure most probably the  $g_{9/2}$  alignment appears at this frequency. Contrary to the calculated curves, the experimental values show a

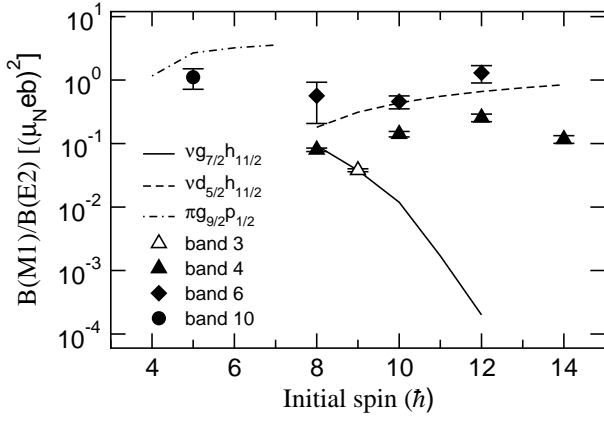


FIG. 6: Experimental and calculated  $B(M1)/B(E2)$  ratios of bands 3, 4, 6 and 10.

more gradual change in  $I_x$  at an  $\sim 50\text{--}70$  keV/ $\hbar$  higher frequency, as it is visible in Fig. 5. This discrepancy might be caused by a larger deformation than  $\beta_2 \approx 0.15$  and  $\gamma \approx -2^\circ$  derived from the TRS calculations similarly as it was suggested in the case of  $^{102}\text{Ru}$  [12].

The alignment behaviour of bands 5 and 6 seems to be similar to bands 3 and 4 as it is presented in Fig. 3. According to the TRS calculations, one quasineutron placed in the E  $h_{11/2}$  orbitals and the other one in the C or D  $d_{5/2}$ ,  $g_{7/2}$  orbitals can account for the next lowest energy negative-parity configurations. Since the experimental  $E'$  curves are in a good agreement with the TRS Routhians (see Fig. 4), we propose a  $\nu h_{11/2}$ , ( $d_{5/2}, g_{7/2}$ ) configuration for bands 5 and 6. For the CE and DE states the calculations predict a  $\beta_2 \approx 0.17$  deformation and a small  $\gamma \approx 7^\circ$  triaxiality similarly to the AE and BE  $\nu h_{11/2}$ , ( $d_{5/2}, g_{7/2}$ ) states. It is worth mentioning that the experimental aligned angular momentum values of bands 5 and 6 show a sharper  $\pi g_{9/2}$  alignment than those of the other two negative parity bands. The observed alignment frequency overlaps with the  $\sim 0.53$  MeV/ $\hbar$  calculated one, as it can be seen in Fig. 5. As band 1 shows a similar behaviour at about this frequency, it is supposed to correspond to the alignment of a  $g_{9/2}$  quasiproton pair, too.

The  $B(M1)/B(E2)$  ratios within a  $\Delta I = 1$  band are sensitive to the quasiparticle configuration of the band. Thus, to corroborate the configuration assignments of the negative-parity bands, we deduced the experimental  $B(M1; I \rightarrow I-1)/B(E2; I \rightarrow I-2)$  ratios of reduced transition probabilities from the measured  $I_\gamma(M1)/I_\gamma(E2)$  branching ratios for bands 3, 4 and 6. Since there is no observed M1 transition in band 5 to the corresponding signature partner, reduced transition probability ratios could not be obtained for it. The  $B(M1)/B(E2)$  ratios were extracted using the expression

$$\begin{aligned} \frac{B(M1; I \rightarrow I-1)}{B(E2; I \rightarrow I-2)} &= \\ &= 0.697 \frac{E_\gamma^5(E2)}{E_\gamma^3(M1)} \frac{I_\gamma(M1)}{I_\gamma(E2)} \frac{1}{1 + \delta^2} \left( \frac{\mu_N}{eb} \right)^2, \end{aligned} \quad (2)$$

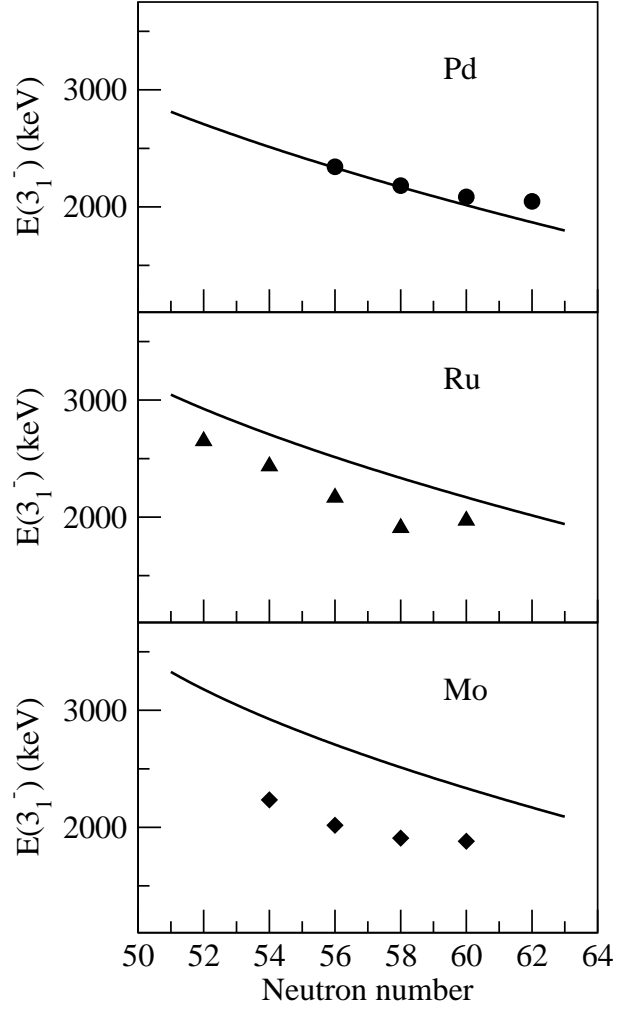


FIG. 7: Energies of the first  $3^-$  states in Mo, Ru and Pd isotopes compared to the curves obtained from eq. 3. The data for  $^{96\text{--}108}\text{Ru}$  and  $^{102,106\text{--}110}\text{Pd}$  are taken from [29–37].

where the energies of the  $\gamma$  rays are given in MeV. The branching ratios were determined by setting gates on the transitions above the decaying level. The  $\delta$ -multipole mixing ratios of the  $\Delta I=1$  transitions were assumed to be small, and thus  $\delta^2$  can be neglected. The experimental  $B(M1)/B(E2)$  ratios were compared to calculated values obtained as it is described in details in Ref. [12].

The experimental  $B(M1)/B(E2)$  ratios for bands 3, 4 and 6 are plotted in Fig. 6 together with the calculated values. The observed  $B(M1)/B(E2)$  ratios fall between the theoretical curves corresponding to  $\nu d_{5/2}h_{11/2}$  and  $\nu g_{7/2}h_{11/2}$  configurations, somewhat closer to the former one, which further strengthens the proposed two-quasineutron structure of the negative parity bands.

### C. The low-spin negative-parity states

In the regions of nuclei with neutron or proton number near 34, 56 and 88 strong octupole effects are expected, since the Fermi surface is between the  $g_{9/2}-p_{3/2}$ ,  $h_{11/2}-d_{5/2}$  and  $i_{13/2}-f_{7/2}$  orbitals [38], respectively. Accordingly, the appearance of octupole structure can be expected for  $^{104}\text{Pd}$  having 58 neutrons. One of the fingerprints of octupole correlation is the presence of a low-lying  $3^-$  collective state. Indeed, a  $3^-$  state is observed at 2182 keV in  $^{104}\text{Pd}$ , the octupole character of which can be tested using a simple parametrization established by Zamfir *et al.* for the energies of  $3_1^-$  states in all nuclei with  $A > 30$  [39]:

$$E(3_1^-) = 19A^{-1/3} - 0.5\sqrt{N_p + N_n}, \quad (3)$$

where  $E(3_1^-)$  is obtained in MeV,  $N_p$  and  $N_n$  are the valence-proton and -neutron numbers, respectively. Differences from the curve characterizing the normal behavior nuclei indicate octupole correlations. In Fig. 7 the energies of the first  $3^-$  states in Mo, Ru and Pd nuclei are compared to the curves derived for the corresponding isotope chains. The valence-proton numbers  $N_p$  were counted from the  $Z = 40$  sub-shell closure, while the valence-neutron numbers  $N_n$  were taken from the  $N = 50$  shell closure. In the case of Mo nuclei the experimental energies fall below the calculated curve by  $\sim 600$ -700 keV in agreement with the presence of octupole collectivity observed in  $^{98,100,102}\text{Mo}$  [40]. For Ru isotopes the deviations decrease and for Pd nuclei the experimental values lie close to the calculated curve. On the basis of this fact the  $3_1^-$  state in  $^{104}\text{Pd}$  may not be connected to octupole correlations.

In the interpretation of the closely spaced  $3^-$ ,  $4^-$  and  $5^-$  states at 2182, 2298 and 2492 keV another hint can be obtained from the  $i_x$  experimental alignments (see in Fig. 3). Compared to the yrast band *band 10* shows an alignment gain of  $\sim 4 \hbar$ , so it is assumed to be configured by two quasiparticles. As more two-quasineutron structures are not expected below *bands 3, 4, 5, 6* belonging to the  $\nu h_{11/2}, (d_{5/2}, g_{7/2})$  configurations, *band 10* can be built on two-quasiproton configurations. Indeed, similar structures have been found in  $N = 44$  isotones  $^{78}\text{Se}$ ,  $^{80}\text{Kr}$ ,  $^{82}\text{Sr}$  and  $^{84}\text{Zr}$  [41–45], and assigned to non-collective  $\nu g_{9/2}, (p_{1/2}, f_{5/2})$  configurations [41]. In Pd isotopes with proton number  $Z = 46$  analogous two-quasiproton excitations can be expected.

In  $^{103}\text{Rh}$ , the odd- $Z$  neighbour of  $^{104}\text{Pd}$ , bands built on the ground state and the low-lying isomer state have been observed and assigned to the  $\pi p_{1/2}$  and  $\pi g_{9/2}$  one-quasiproton configurations [46], respectively. The  $5/2_1^-$  state related to the  $\pi f_{5/2}$  configuration has been found at a higher excitation energy of 880 keV [46]. Accordingly, the  $\pi g_{9/2}$  and the  $\pi p_{1/2}$  orbits should be close to the Fermi surface also in  $^{104}\text{Pd}$ , and the lowest-lying two-quasiproton excitations are expected to belong to the  $\pi g_{9/2}p_{1/2}$  configuration, while the  $\pi g_{9/2}f_{5/2}$  structures

are assumed to appear at higher excitation energies of about 800 keV. Thus, we propose the  $\pi g_{9/2}p_{1/2}$  two-quasiproton configuration tentatively to these low-lying negative-parity states.

In the TRS calculations the lowest-energy negative-parity two-quasiproton configurations are predicted to be built on one quasiproton from the  $a$  and  $b$   $g_{9/2}$  orbitals and another quasiproton from the  $e$  and  $f$   $p_{1/2}$  orbitals. The explanation of the labelling of quasiproton states is given in Table II. The reasonable agreement between the experimental and the TRS Routhians and aligned angular momenta, presented in Fig. 4 and 5, strengthens the  $\pi g_{9/2}p_{1/2}$  configuration assignment to *band 10*. For these states the calculations predict a shape with  $\beta_2 \approx 0.15$  and  $\gamma \approx -10^\circ$ .

In the case of *band 10* we could extract the experimental  $B(M1)/B(E2)$  ratio only for one excited state placed at 2492 keV. The obtained ratio is presented in Fig. 6 together with the calculated curve corresponding to the  $\pi g_{9/2}p_{1/2}$  configuration. In the calculations we applied 0.5 and 1.1  $g$ -factors for the  $\pi p_{1/2}$  and the  $\pi g_{9/2}$  configurations, respectively, obtained from the magnetic moments  $\mu$  of the corresponding states in  $^{103}\text{Rh}$  [46]. The  $\beta_2$  and  $\gamma$  shape parameters were chosen according to the TRS predictions, while the signature splitting was not taken into account in the calculations. Further details of the analysis are described above in Sec. B. Comparing the experimental and the calculated values, the observed  $B(M1)/B(E2)$  ratio lies close to the theoretical curve of the  $\pi g_{9/2}p_{1/2}$  configuration, which further supports the proposed two-quasiproton structure of *band 10*.

### D. The B(E1) transition strengths

Although the  $3_1^-$  state in  $^{104}\text{Pd}$  does not show origin of permanent octupole deformation, in the case of the negative-parity bands the excitation of  $h_{11/2}$  neutrons may induce some octupole correlations. In  $^{100}\text{Pd}$  signs of octupole collectivity have been found at negative-parity higher-spin states [47]. In nuclei with neutron numbers above  $N = 50$  one of the lowest-energy positive-parity orbital is the  $\nu d_{5/2}$ , and hence, the excitations into the  $\nu h_{11/2}$  orbital are favoured by coupling to the octupole phonon [48]. The observation of enhanced  $\Delta I=1$  E1 transitions would indicate the presence of octupole collectivity [49], therefore we analysed the relevant transitions from this respect.

Since the E1 operator connects states from two different shells, they are always very hindered. In the  $A = 100$  mass region the single-proton E1 transitions are hindered by a factor of  $1-3 \times 10^{-6}$  in odd Ag and In isotopes, while the single-neutron transitions are hindered by a factor of  $1-2 \times 10^{-5}$  in odd Cd isotopes.

The  $B(E1)$  values for the E1 linking transitions between *bands 2* and *3* were estimated from the  $I_\gamma(E1)/$

TABLE III: The reduced E1 transition probabilities in  $^{104}\text{Pd}$  estimated from branching ratios compared to known values in  $^{100}\text{Pd}$  and  $^{117,119}\text{Cd}$ .

Nucleus	$E_\gamma(\text{keV})$	$I_i^\pi \rightarrow I_f^\pi$	$B(E1)(\text{W.u.})$
$^{104}\text{Pd}$	655	$10^+ \rightarrow 9^-$	$6.3(8) \times 10^{-5}$
	588	$12^+ \rightarrow 11^-$	$3.1(2) \times 10^{-5}$
	469	$14^+ \rightarrow 13^-$	$3.4(8) \times 10^{-5}$
$^{100}\text{Pd}$	994		$1.5(3) \times 10^{-5}$
	718		$3.9(3) \times 10^{-5}$
	908		$1.4(3) \times 10^{-5}$
	591		$5.1(4) \times 10^{-5}$
	998		$1.6(4) \times 10^{-5}$
	786		$3.2(4) \times 10^{-5}$
	706		$1.2(2) \times 10^{-4}$
$^{117}\text{Cd}$	205		$2.0(2) \times 10^{-5}$
	220		$9.4(9) \times 10^{-6}$
$^{119}\text{Cd}$	199		$1.1(1) \times 10^{-5}$
	213		$9.4(2) \times 10^{-6}$

$I_\gamma(E2)$  branching ratios using the following expression:

$$\frac{B(E1; I \rightarrow I-1)}{B(E2; I \rightarrow I-2)} = \frac{1}{1.3 \times 10^6} \frac{E_\gamma^5(E2)}{E_\gamma^3(E1)} \frac{I_\gamma(E1)}{I_\gamma(E2)} (fm^{-2}), \quad (4)$$

where the energies of the  $\gamma$  rays are given in MeV. The  $B(E2)$  values were calculated as

$$B(E2; I \rightarrow I-2) = \frac{5}{16\pi} Q_0^2 | \langle J_i K 2 0 | J_f K \rangle |^2, \quad (5)$$

where  $K = 1$  and  $Q_0 = 2$  eb values obtained from the prediction of the TRS calculations for *band 3* were used.

It can be seen from the deduced  $B(E1)$  probabilities given in Table III that the hindrance factors are about  $3-6 \times 10^5$ . As *band 3* shows two-quasineutron character, the obtained values are to be compared to those known in Cd isotopes. On the basis of this comparison the E1 transitions observed in  $^{104}\text{Pd}$  are only slightly enhanced, if they are enhanced at all. The deduced low values of enhancement mean that signs of octupole correlations were not found in  $^{104}\text{Pd}$ .

### E. The quasi- $\gamma$ bands 7 and 8

Low-lying cascades built on the second  $2^+$  state have been observed in several Pd and Ru isotopes in the  $A \approx 100$  mass region. Recently, such a structure has been identified also in  $^{102}\text{Ru}$  and it was interpreted as a quasi- $\gamma$  band associated with  $\gamma$ -soft triaxial deformation, which might be confined in a region away from axial symmetry [5]. Since the nuclear structure of  $^{104}\text{Pd}$  shows similar characteristics than that of  $^{102}\text{Ru}$  having only 2 protons less, the existence of a quasi- $\gamma$  band is expected also in the studied nucleus.

The levels of the non-yrast low-lying positive-parity *bands 7* and *8* established in the present work were grouped into a  $\gamma$ -band which is built on the second  $2^+$

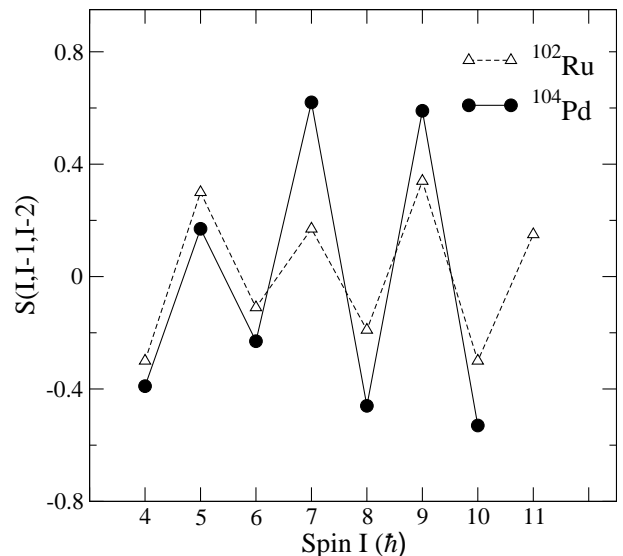


FIG. 8: Experimentally observed odd-even spin energy staggering in *bands 7* and *8* (filled circles, solid line) compared to the values of the quasi- $\gamma$  band in  $^{102}\text{Ru}$  (opened triangles, solid line) [5]. The lines between the symbols are drawn to guide the eye.

state at 1342 keV. The band assignment is based on the observed decay pattern and on the similarities with the structure of  $^{102}\text{Ru}$ . A distinction between excitations in a  $\gamma$ -soft and a  $\gamma$ -rigid potential can be deduced from the energy sequence in the  $\gamma$ -band and can be expressed in the odd-even spin energy staggering function

$$S(I, I-1, I-2) = \frac{E(I) + E(I-2) - 2E(I-1)}{E(2_1^+)}. \quad (6)$$

In the case of a triaxial rigid rotor this staggering gives positive values for even spins and negative ones for odd spins. For a  $\gamma$ -soft rotor it has an opposite phase, the values fall below 0 for even spins and above 0 for odd spins.

The experimental odd-even spin energy staggering deduced for *bands 7* and *8* are displayed in Fig. 8 together with the values extracted for  $^{102}\text{Ru}$  [5]. The values obtained for  $^{104}\text{Pd}$  are in the same order of magnitude as in  $^{102}\text{Ru}$ . They vary between the negative values of  $-0.23$  and  $-0.53$  for even spins and they fall between the positive values of  $0.17$  and  $0.62$  for odd spins. The resulted phase of the staggering is the same both in  $^{104}\text{Pd}$  and  $^{102}\text{Ru}$ . Accordingly to the obtained odd-even spin energy staggering in  $^{104}\text{Pd}$ , we can rule out the rigid triaxial rotor scenario and assign a  $\gamma$ -soft character to this nucleus. It is worth mentioning that the size of the staggering is about the same at the bottom part of the  $\gamma$ -bands both in  $^{104}\text{Pd}$  and  $^{102}\text{Ru}$ , while it increases at higher spins of

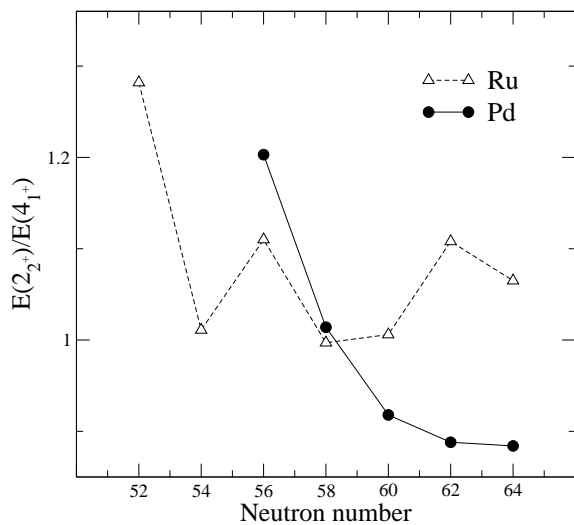


FIG. 9: Energy ratios  $E(2_2^+)/E(4_1^+)$  deduced for Pd and Ru isotopes. The data for  $^{96-108}\text{Ru}$  and  $^{102,106-110}\text{Pd}$  are taken from [29–36]. The lines between the symbols are drawn to guide the eye.

$^{104}\text{Pd}$  unlike  $^{102}\text{Ru}$ . It might indicate a more  $\gamma$ -soft shape at the higher spin region in  $^{104}\text{Pd}$  compared to  $^{102}\text{Ru}$ .

The  $\gamma$ -softness in the Pd and Ru isotopes can be compared by deducing the energy ratio  $E(2_2^+)/E(4_1^+)$ . In terms of the  $\gamma$ -fluctuating triaxial rotor model [41, 50] the  $\gamma$ -softness of the potential is represented by the energy of the second  $2^+$  state relative to that of the yrast  $4^+$  state: the softer the nucleus, the lower is the  $2_2^+$  state relative to the  $4_1^+$  one. The ratios  $E(2_2^+)/E(4_1^+)$  obtained for Pd and Ru isotopes between neutron numbers  $N = 52$  and 64 are presented in Fig. 9. In the case of Ru isotopes the degree of  $\gamma$ -softness seems to remain about the same above  $N = 54$ . For Pd isotopes the observed curve indicates increasing  $\gamma$ -softness with increasing neutron number crossing the pattern of Ru nuclei at  $N = 58$ . Above this neutron number this feature can cause a difference in the possible formation of chiral structures in Ag and Rh nuclei, of which Pd and Ru isotopes serve as cores,

respectively.

#### IV. SUMMARY

High-spin states of  $^{104}\text{Pd}$  were studied via the  $^{96}\text{Zr}(^{13}\text{C},5n)$  reaction using the EUROBALL IV  $\gamma$ -ray spectrometer coupled with the DIAMANT array for the detection of charged particles. All earlier known bands were extended significantly and additional bands were identified. On the basis of the deduced  $B(M1)/B(E2)$  ratios and the comparison of the experimental Routhians and aligned angular momenta to the predictions of Woods-Saxon TRS calculations,  $\nu h_{11/2}, (d_{5/2}, g_{7/2})$  two-quasineutron configuration was assigned to the high-spin negative-parity bands. Two-quasiproton structures were found the first time in this mass region, the low-spin negative-parity states were identified belonging to the  $\pi g_{9/2}p_{1/2}$  configuration. The non-yrast low-lying positive-parity bands, also observed in this work for the first time, were interpreted as excitations associated with  $\gamma$ -soft deformation on the basis of their energy staggering as a function of spin.

#### Acknowledgments

This work was supported in part by the European Community - Access to Research Infrastructures action of the Improving Human Potential Programme (contract EUROVIV: HPRI-CT-1999-00078), the Hungarian Scientific Research Fund OTKA (contract number K72566), the Natural Sciences and Engineering Research Council of Canada under Contract No. SAPIN/371656-2010, the Bolyai János Foundation of HAS, the FPA 2002-04181-C04-03, the US National Science Foundation, the US Department of Energy, and the UK Engineering and Physical Sciences Research Council. The work is supported by the TÁMOP-4.2.2/B-10/1-2010-0024 project. The project is co-financed by the European Union and the European Social Fund.

- 
- [1] S. Chattopadhyay *et al.*, Phys. Rev. **C 57**, R471 (1998); J. Timár *et al.*, Nucl. Phys. **A 696**, 241 (2001); J. Gizon *et al.*, Nucl. Phys. **A 658**, 97 (1999); J. Timár *et al.*, Acta Phys. Pol. B **33**, 493 (2002); R.-R. Zheng *et al.*, Chin. Phys. Lett. **21**, 1475 (2004).
- [2] C. Vaman *et al.*, Phys. Rev. Lett. **92**, 032501 (2004).
- [3] J. Timár *et al.*, Phys. Lett. **B598**, 178 (2004).
- [4] P. Joshi *et al.*, Phys. Lett. **B595**, 135 (2004).
- [5] S. Lalkovski *et al.*, Phys. Rev. **C 71**, 034318 (2005).
- [6] J. Timár *et al.*, Phys. Rev. **C 73**, 011301(R) (2006).
- [7] D. Tonev *et al.*, Phys. Rev. Lett. **96**, 052501 (2006).
- [8] J. Srebrny *et al.*, Acta Phys. Pol. **36**, 1063 (2005).
- [9] T. Suzuki *et al.*, Phys. Rev. **C 78**, 031302(R) (2008).
- [10] J. Timár *et al.*, Phys. Rev. **C 76**, 024307 (2007).
- [11] P. Joshi *et al.*, Phys. Rev. Lett. **98**, 102501 (2007).
- [12] D. Sohler *et al.*, Phys. Rev. **C 71**, 064302 (2005).
- [13] J.A. Grau *et al.*, Phys. Rev. **C 14**, 2297 (1976).
- [14] D.C. Stromswold *et al.*, Phys. Rev. **C 13**, 1510 (1976).
- [15] A.O. Macchiavelli *et al.*, Phys. Rev. **C 38**, 1088 (1988).
- [16] J. Simpson, Z. Phys. **A358**, 139 (1997).
- [17] J. Eberth *et al.*, Nucl. Instr. Meth. **A369**, 135 (1996).
- [18] G. Duchêne *et al.*, Nucl. Instr. Meth. **A432**, 90 (1999).
- [19] J.N. Scheurer *et al.*, Nucl. Instr. and Meth. **A 385**, 501 (1997).
- [20] D.C. Radford, Nucl. Instr. Meth. **A 361**, 297 (1995).
- [21] A. Krämer-Flecken *et al.*, Nucl. Instrum. Methods **A 275**, 333 (1989).
- [22] P.M. Jones *et al.*, Nucl. Instrum. Methods **A 362**, 556

- (1995).
- [23] W. Nazarewicz *et al.*, Nucl. Phys. **A 467**, 437 (1987).
- [24] W. Nazarewicz *et al.*, Nucl. Phys. **A 503**, 285 (1989).
- [25] R. Wyss *et al.*, Phys. Lett. **215B** 211, (1988).
- [26] R. Bengtsson and S. Frauendorf, Nucl. Phys. **A 327**, 139 (1979).
- [27] B.M. Nyakó *et al.*, Phys. Rev. **C 60**, 024307 (1999).
- [28] F.A. Rickey *et al.*, Phys. Rev. **C 15**, 1530 (1977).
- [29] D. Abriola and A.A. Sonzogni, Nucl. Data Sheets **109**, 2501 (2008).
- [30] Balraj Singh and Zhiqiang Hu, Nucl. Data Sheets **98**, 335 (2003).
- [31] Balraj Singh, Nucl. Data Sheets **109**, 297 (2008).
- [32] D. de Frenne, Nucl. Data Sheets **110**, 1745 (2009).
- [33] J. Blachot, Nucl. Data Sheets **108**, 2035 (2007).
- [34] D. de Frenne and A. Negret, Nucl. Data Sheets **109**, 943 (2008).
- [35] J. Blachot, Nucl. Data Sheets **91**, 135 (2000).
- [36] D. de Frenne and E. Jacobs, Nucl. Data Sheets **89**, 481 (2000).
- [37] H. Klein *et al.*, Phys. Rev. **C 65**, 044315 (2002).
- [38] P.A. Butler and W. Nazarewicz, Rev. Mod. Phys. **C 68**, 349 (1996).
- [39] N.V. Zamfir *et al.*, Phys. Lett. **B226**, 11 (1989).
- [40] S. Lalkovski *et al.*, Phys. Rev. **C 75**, 014314 (2007).
- [41] J. Döring *et al.*, Phys. Rev. **C 67**, 014315 (2003).
- [42] R. Schwengner *et al.*, Z. Phys. A **326**, 287 (1987).
- [43] L. Funke *et al.*, Nucl. Phys. **A355**, 228 (1981).
- [44] J. Döring *et al.*, Phys. Rev. **C 52**, 76 (1995).
- [45] S.L. Tabor *et al.*, Phys. Rev. **C 49**, 730 (1994).
- [46] D. De Frenne, Nucl. Data Sheets **110**, 2081 (2009).
- [47] D. Sohler *et al.*, Nucl. Phys. **A 686**, 41 (2001).
- [48] G. de Angelis *et al.*, Phys. Lett. **B437**, 236 (1998).
- [49] P.A. Butler, W. Nazarewicz, Rev. Mod. Phys. **68**, 349 (1996).
- [50] N. Onishi *et al.*, Nucl. Phys. **A452**, 71 (1986).